American Mineralogist, Volume 96, pages 878–887, 2011

Ambrinoite, $(K,NH_4)_2(As,Sb)_8S_{13}\cdot H_2O$, a new mineral from Upper Susa Valley, Piedmont, Italy: The first natural (K,NH_4)-hydrated sulfosalt

Cristian Biagioni,[1] Elena Bonaccorsi,[1,2,*] Marco Pasero,[1] Yves Moëlo,[3] Marco E. Ciriotti,[4] Danilo Bersani,[5] Athos Maria Callegari,[6] and Massimo Boiocchi[7]

[1]Dipartimento di Scienze della Terra, Università di Pisa, Via Santa Maria 53, I-56126 Pisa, Italy
[2]Istituto di Geoscienze e Georisorse, CNR, Via Moruzzi 1, I-56124 Pisa, Italy
[3]Institut des Matériaux Jean Rouxel (IMN), Université de Nantes, CNRS, 2, rue de la Houssinière, BP 32229, F-44322 Nantes Cedex 3, France
[4]Associazione Micromineralogica Italiana, Via San Pietro 55, I-10073 Devesi-Ciriè, Italy
[5]Dipartimento di Fisica, Università di Parma, Viale G.P. Usberti 7/a, I-43100 Parma, Italy
[6]Dipartimento di Scienze della Terra, Università di Pavia, Via Ferrata 1, I-27100 Pavia, Italy
[7]Centro Grandi Strumenti, Università di Pavia, Via Bassi 21, I-27100 Pavia, Italy

Abstract

Ambrinoite, ideally $(K,NH_4)_2(As,Sb)_8S_{13}\cdot H_2O$, occurs as a rare sulfosalt species in the Triassic evaporitic formation of *Gessi* (gypsum) outcropping near the hamlet of Signols (Oulx, Susa Valley, Torino, Piedmont, Italy). The new species is associated with sulfur and orpiment; in the same occurrence galkhaite, stibnite, and enargite were also identified. Ambrinoite occurs as aggregates of tabular crystals up to 1 mm in length. The color is red, with an orange-red streak; the luster is vitreous to resinous. The mineral is transparent; its microhardness $VHN_{(10\ g)}$ = 30 kg/mm^2, corresponding to a Mohs hardness of about 2. Electron microprobe analysis gives the empirical formula $[K_{1.43}(NH_4)_{0.42}Na_{0.02}Tl_{0.01}]_{\Sigma=1.88}(As_{5.82}Sb_{2.18})_{\Sigma=8.00}S_{13.22}\cdot 1.2H_2O$, close to stoichiometric $[K_{1.5}(NH_4)_{0.5}]_{\Sigma=2}(As_6Sb_2)_{\Sigma=8}S_{13}\cdot H_2O$; the calculated density is 3.276 g/cm^3. Micro-Raman spectroscopy confirmed the presence of water and ammonium cation. Ambrinoite is triclinic, space group $P\bar{1}$, with a = 9.704(1), b = 11.579(1), c = 12.102(2) Å, α = 112.82(1), β = 103.44(1), γ = 90.49(1)°, V = 1211.6(3) Å^3, Z = 2. The strongest X-ray powder diffraction lines [d in Å (I) (hkl)] are: 10.78 (100) (001), 5.79 (55) ($0\bar{2}1$), 4.23 (35) (102), 5.31 (34) ($\bar{1}02$), 5.39 (32) (002). Its crystal structure has been solved by X-ray single-crystal diffraction on the basis of 2667 unique reflections, with a final R = 0.035. It is formed by two kinds of modules: slabs $(110)_{PbS}$ of modified PbS archetype (type A slabs) and openwork slabs with channels accomodating $(K,NH_4)^+$ cations and H_2O molecules (type B slabs). Its structure can be described as an order-disorder (OD) structure, built up by two different kinds of layers. Taking into account only the short (As,Sb)-S bonds, $(As,Sb)S_3$ triangular pyramids form double chains similar to those described in other natural and synthetic compounds, among which its homeotype gillulyite, as well as gerstleyite. Ambrinoite belongs to the hutchinsonite merotypic family. It is probably the product of late-stage hydrothermal fluid circulation. The name of this new mineral species (IMA 2009-071) honors Pierluigi Ambrino (b. 1947), the mineral collector who kindly provided us with the studied specimens.

Keywords: Ambrinoite, sulfosalt, potassium, ammonium, crystal structure, gillulyite, Signols, Upper Susa Valley, Torino, Piedmont, Italy

Introduction

The Upper Susa Valley (Piedmont, Italy) is characterized by the relative abundance of evaporitic outcrops, belonging to the Triassic "*Gessi*" (gypsum) formation. These evaporites, which are part of the Pennidic Domain, are usually associated with detachment horizons separating ophiolitic and oceanic units from continental units. In particular, in the area of Signols, the Gessi formation is located between the ophiolitic units of Roche de l'Aigle and of Vin Vert, and the continental units of Vallonetto and Ambin (Polino 1999).

The mineralogy of these evaporitic rocks was studied by Colomba (1898, 1909), who described the presence of anhydrite, dolomite, gypsum, halite, hematite, a (Li,Mg)-rich mica, pyrite, quartz, sphalerite, sulfur, and tourmaline. Damarco and Barresi (2005) reported also the occurrence of fluorite, orpiment, and stibnite. Finally, Biagioni et al. (2010) described the findings of enargite and of the very rare sulfosalt galkhaite.

The aim of this paper is the description of ambrinoite, a new sulfosalt from Upper Susa Valley. The new species and its name have been approved by the CNMNC of the IMA (no. 2009-071). It is named after Pierluigi Ambrino (b. 1947), the mineral collector who provided us with the studied specimens. The type material is deposited in the mineralogical collection of the Museo di Storia Naturale e del Territorio, University of Pisa, under the catalog number 19500; the cotype specimen is deposited in the mineralogical collection of the Museo Regionale di Scienze Naturali, Torino, with catalog number M/15824.

* E-mail: elena@dst.unipi.it

0003-004X/11/0506–878$05.00/DOI: 10.2138/am.2011.3723

Occurrence and paragenesis

Ambrinoite was found in the Cumbë Sûrdë quarry, Signols, Oulx, Upper Susa Valley, Torino, Piedmont, Italy. This quarry had been exploited for gypsum since 1883 and was abandoned in the early sixties of the 20th Century (Guiguet et al. 2003).

The first specimens of ambrinoite were found in 1998 by the mineral collectors P. Ambrino, A.A. Barresi, and P. Brizio; unfortunately, the very low amount of material did not allow its identification as a new species. In 2007, the mineral collector R. Cola found a new specimen in which the phase was abundant and well crystallized, but he did not recognize the red mineral as a potential new species. He presented the sample by chance to P. Ambrino, who immediately brought it back to the same findings of 1998, and provided us with the sample for a full description.

In hand specimen, ambrinoite occurs as cinnabar-red lamellar aggregates, up to 1 mm thick, scattered in the saccharoidal gypsum matrix, together with sulfur and orpiment. Tabular crystals of this new mineral, elongated on [100], are up to 100 μm long and less than 10 μm across. The paragenesis suggests a low temperature of formation. Besides, as stated above, Biagioni et al. (2010) reported the presence of galkhaite at Signols, in association with orpiment; according to Pekov and Bryzgalov (2006), galkhaite is a low-temperature phase. Therefore, ambrinoite was probably deposited by highly alkaline low-temperature hydrothermal fluids, similarly to the only other hydrated alkaline sulfosalt known in nature, i.e., gerstleyite (Frondel and Morgan 1956), described in the Kramer borate district (California, U.S.A.).

Optical and physical properties

Ambrinoite is cinnabar-red in color, very similar to getchellite; it has a reddish streak and a vitreous to resinous luster. Minute fragments are transparent. In plane polarized transmitted light, ambrinoite shows a strong pleochroism, being yellow along [100] and orange-red in a normal direction. Between crossed polars, the mineral shows a parallel extinction to the cleavage traces and a negative elongation. Birefringence is hidden by the reddish color of the crystals. The mean refractive index was calculated using the method proposed by Korotkov and Atuchin (2008); according to these authors, the average possible error of the calculations for non-oxide compounds is about 12%. Taking into account the chemical formula derived by the structural study (see below), the mean refractive index of ambrinoite should be 2.5(3), but could not be measured.

Density was not measured because of the scarcity of available material; the calculated density, with the same formula used for mean refraction calculation, is 3.276 $g\cdot cm^{-3}$.

Ambrinoite is brittle and its fracture is splintery. It shows two perfect cleavages on {001} and {010}, whereas on {100} the cleavage is poor. Mohs hardness could not be directly measured because of the small crystal size. It is less than 2, according to a measured value VHN (10 g load) of 30 kg/mm^2. This value corresponds to a microhardness of 0.32 GPa, to be compared with 0.14 for talc and 0.61 for gypsum (Broz et al. 2006).

Chemical and spectroscopic studies

In search of an unexpected component: The ammonium cation

The presence of ammonium in ambrinoite was first suspected, then proven, by a feedback process combining electron microprobe analysis, crystal structure solution and micro-Raman spectroscopy. At a first step, preliminary EDS analysis with SEM showed the presence of K, As, Sb, and S as the only significant elements with $Z > 9$. The crystal structure study then indicated a formula close to stoichiometric $K_2(As,Sb)_8S_{13}\cdot H_2O$, but with an unexplained deficit on the occupancy of the K sites (and thus a deficit of positive charges), suggesting the additional presence of another (monovalent) cation, with a lower Z [higher Z would have overpassed a full site occupancy: significant Rb or Cs contents are excluded, despite the occurrence of galkhaite, $(Cs,Tl,\square)(Hg,Cu,Zn)_6(As,Sb)_4S_{12}$, at Signols].

Lithium, Na, or NH_4 were possible candidates. In Signols evaporites, lithium was detected in a (Li,Mg)-rich mica (Colomba 1898); its substitution to K in ambrinoite would contract the mean volume of K sites, but preliminary bond valence calculations on K positions indicate a valence deficit that is inversely an expanded volume, which excludes any significant substitution of K by a smaller cation, Li or Na.

Finally, it was hypothesized that K^+ was partially replaced by NH_4^+, a larger but lighter monovalent cation, as it was reported by Zelenski et al. (2009) for tazieffite, a complex chloro-sulfosalt from Kamtchatka (Russia). In addition, it is known that in evaporitic environments high concentration of ammonium ion, formed by deamination of organic matter during early diagenesis, is common in fluid inclusions (Bogomolov et al. 1970; Pironon et al. 1995a, 1995b). The presence of ammonium was indirectly inferred in tazieffite (Zelenski et al. 2009), but could not be detected, due to its very low expected content (0.03 wt%).

On this basis, ambrinoite was analyzed by a microprobe equipped with WDS, with a program including N, together with Na and Tl. Despite an analytical artifact (see below), N could be detected (with only traces of Na and Tl). Simultaneously, a Raman study of ambrinoite permitted to confirm qualitatively the presence of H_2O molecules together with NH_4^+ ions.

Electron microprobe analysis

Three crystal fragments of ambrinoite were prepared as a polished section. Chemical analysis was performed with a CAMEBAX SX 100 electron microprobe (West Microprobe Laboratory, IFREMER, Plouzané, France). The operating conditions were: accelerating voltage 20 kV (10 kV for oxygen and nitrogen), beam current 20 nA, beam size 5 μm, a short counting time (10 s) for all elements (to reduce the risk of sample degradation under the beam); standards (element, emission line): orthoclase ($KK\alpha$), albite ($NaK\alpha$), lorandite ($TlM\alpha$), GaAs ($AsL\alpha$), stibnite ($SbL\alpha$), pyrite ($SK\alpha$), and cassiterite ($OK\alpha$). Selenium, Cl, and Hg were planned, but not detected. Nitrogen analysis was performed according to the conditions described by Huneau et al. (2000): synthetic VN as a standard, with $NK\alpha$ line; the short counting time induced a high variability of the N concentration for one spot analysis.

The presence of N was initially overlooked, as the measure of its background was overestimated due to a Sb secondary peak close to the $NK\alpha$ peak. Fortunately, the analysis of orpiment, As_2S_3, getchellite, $AsSbS_3$, and stibnite, Sb_2S_3, as internal standards, allowed to interpolate the true background for N at its peak position in ambrinoite, taking into account its As/Sb ratio. This permitted to reveal a positive difference between peak and background for N in ambrinoite, corresponding to a significant

N content, despite its low values (around 0.5 wt%).

Table 1 gives weight concentrations obtained on the main fragment. For getting the true total, the H content corresponding to H_2O and NH_4^+ was added. There are only traces of Na (mean ~0.05 wt%) and Tl (mean ~0.13 wt%), whereas N is close to 0.5 wt%. Oxygen reaches 1.5 wt%. Table 1 (lower part) gives atom ratios on the basis of (As + Sb) = 8 atoms. Taking into account the N content as NH_4^+ cation, the valence equilibrium *Ev* appears good (mean: –1.9%). The sum of monovalent cations is in agreement with the total of 2 apfu, as suggested by the structural results; it thus excludes a significant content of Li (which cannot be detected by EPMA). Potassium concentration is very homogeneous (1.43 ± 0.02 apfu), indicating that fluctuations in N atom ratio (0.42 ± 0.14 apfu) are due exclusively to a poor count statistic. Although N concentration is only about the tenth of that of K, the NH_4/K atom ratio is very high, close to 0.3. The As/Sb ratio is close to 6:2, with a significant As-for-Sb substitution, from ($As_{6.1}Sb_{1.9}$) to ($As_{5.45}Sb_{2.55}$).

The mean structural formula of the analyzed fragment is

$$[K_{1.43}(NH_4)_{0.42}Na_{0.02}Tl_{0.01}]_{\Sigma=1.88}(As_{5.82}Sb_{2.18})_{\Sigma=8.00}S_{13.22}\cdot 1.2H_2O.$$

Taking into account relative errors, especially on light elements O and N, this formula can be idealized as the stoichiometric one

$$[K_{1.5}(NH_4)_{0.5}]_{\Sigma=2}(As_6Sb_2)_{\Sigma=8}S_{13}\cdot H_2O, \text{ or } (K,NH_4)_2(As,Sb)_8S_{13}\cdot H_2O.$$

Micro-Raman spectroscopy

Nonpolarized micro-Raman spectra were obtained on an unpolished fragment of ambrinoite in nearly backscattered geometry with a Jobin-Yvon Horiba "Labram" apparatus, equipped with a motorized *x-y* stage and an Olympus microscope with a 50× objective. The 632.8 nm line of a He-Ne laser was used; laser power was controlled by means of a series of density filters. The minimum lateral and depth resolution was set to a few micrometers. The system was calibrated using the 520.6 cm^{-1} Raman band of silicon before each experimental session. Spectra were collected with multiple acquisitions (2 to 6) with single counting times, ranging between 20 and 180 s. The Raman spectra confirmed the presence of both H_2O and NH_4^+ in the ambrinoite structure. The following lines were observed:

(1) In the region 200–1200 cm^{-1}: 207, 216, 294, 324, 341, 352, 364, 371, and 393 cm^{-1}. These lines can be attributed to As-S and Sb-S stretching and bending vibrations, which occur between 200 and 400 cm^{-1} (Forneris 1969; Kharbish et al. 2007) (Fig. 1a).

(2) In the region between 1200 and 1900 cm^{-1}: 1423 cm^{-1} (N-H bending) and 1595 cm^{-1} (O-H bending) (Fig. 1b).

(3) In the region 2600–3800 cm^{-1}: 3150 cm^{-1} (N-H stretching) and 3475 cm^{-1} (O-H stretching) (Fig. 1c).

These complementary results of the microprobe and Raman studies thus permitted to refine the crystal structure of ambrinoite with a full occupancy of the K sites. (CIF on deposit[1].)

X-RAY DIFFRACTION STUDIES

X-ray powder diffraction

The powder X-ray diffraction pattern for ambrinoite (Table 2) was obtained using a 114.6 mm diameter Gandolfi camera, with Ni-filtered Cu*K*α radiation. Indexing of the reflections was done using the calculated powder pattern obtained by the structural model described below, using the software POWDERCELL (Kraus and Nolze 2000). The unit-cell parameters refined through least-square methods of all the 37 univocally indexed reflections with CELREF

[1] Deposit item AM-11-029, CIF. Deposit items are available two ways: For a paper copy contact the Business Office of the Mineralogical Society of America (see inside front cover of recent issue) for price information. For an electronic copy visit the MSA web site at http://www.minsocam.org, go to the *American Mineralogist* Contents, find the table of contents for the specific volume/issue wanted, and then click on the deposit link there.

TABLE 1. Microprobe analyses of ambrinoite: chemical composition as wt% (upper part) and number of atoms on the basis of 8 (As + Sb) (lower part)

wt%	K	Na	Tl	N	As	Sb	S	O	H_{calc}	Total
1	4.51	0.02	0.01	0.32	37.87	19.23	35.02	1.30	0.25	98.53
2	4.71	0.06	0.16	0.21	37.49	19.31	34.85	1.53	0.25	98.58
3	4.66	0.07	0.14	0.52	37.16	19.42	34.97	1.40	0.32	98.67
4	4.60	0.06	0.17	0.44	37.54	19.87	35.20	1.47	0.31	99.67
5	4.54	0.04	0.09	0.33	36.57	20.48	34.73	1.47	0.28	98.53
6	4.51	0.06	0.07	0.47	35.01	22.63	34.82	1.58	0.33	99.48
7	4.56	0.05	0.20	0.73	34.85	22.64	34.36	1.62	0.41	99.42
8	4.60	0.03	0.16	0.66	34.27	23.55	34.71	1.50	0.38	99.85
9	4.48	0.02	0.20	0.54	33.30	24.77	34.22	1.59	0.35	99.47
10	4.52	0.05	0.07	0.56	32.84	25.04	34.05	1.69	0.37	99.19
mean	4.57	0.05	0.13	0.48	35.69	21.69	34.69	1.52	0.33	99.14
σ	0.07	0.02	0.06	0.16	1.87	2.30	0.37	0.11	0.05	0.51
Atoms	K	Na	Tl	N	As	Sb	S	O	H_{calc}	*Ev**
1	1.39	0.01	0.00	0.28	6.10	1.90	13.17	0.98	3.06	–2.3
2	1.46	0.03	0.01	0.18	6.07	1.93	13.19	1.16	3.06	–2.4
3	1.45	0.04	0.01	0.45	6.05	1.95	13.31	1.07	3.95	–2.2
4	1.42	0.03	0.01	0.38	6.03	1.97	13.22	1.11	3.73	–2.0
5	1.42	0.02	0.01	0.29	5.95	2.05	13.20	1.12	3.39	–2.3
6	1.41	0.03	0.00	0.41	5.72	2.28	13.30	1.21	4.06	–2.5
7	1.43	0.03	0.01	0.64	5.72	2.28	13.17	1.24	5.06	–0.7
8	1.45	0.02	0.01	0.58	5.62	2.38	13.31	1.15	4.62	–1.8
9	1.41	0.01	0.01	0.48	5.49	2.51	13.18	1.23	4.36	–1.5
10	1.44	0.03	0.00	0.50	5.45	2.55	13.19	1.31	4.62	–1.4
mean	1.43	0.02	0.01	0.42	5.82	2.18	13.22	1.16	3.99	–1.9
σ	0.02	0.01	0.00	0.14	0.25	0.25	0.06	0.10	0.69	0.6

* Relative error on the valence equilibrium (%), calculated as [Σ(val+) – Σ(val–)] × 100/Σ(val–). The last decimal digits for the N and O wt% are purely "aesthetic," because the absolute error corresponds to few decimals percentages..

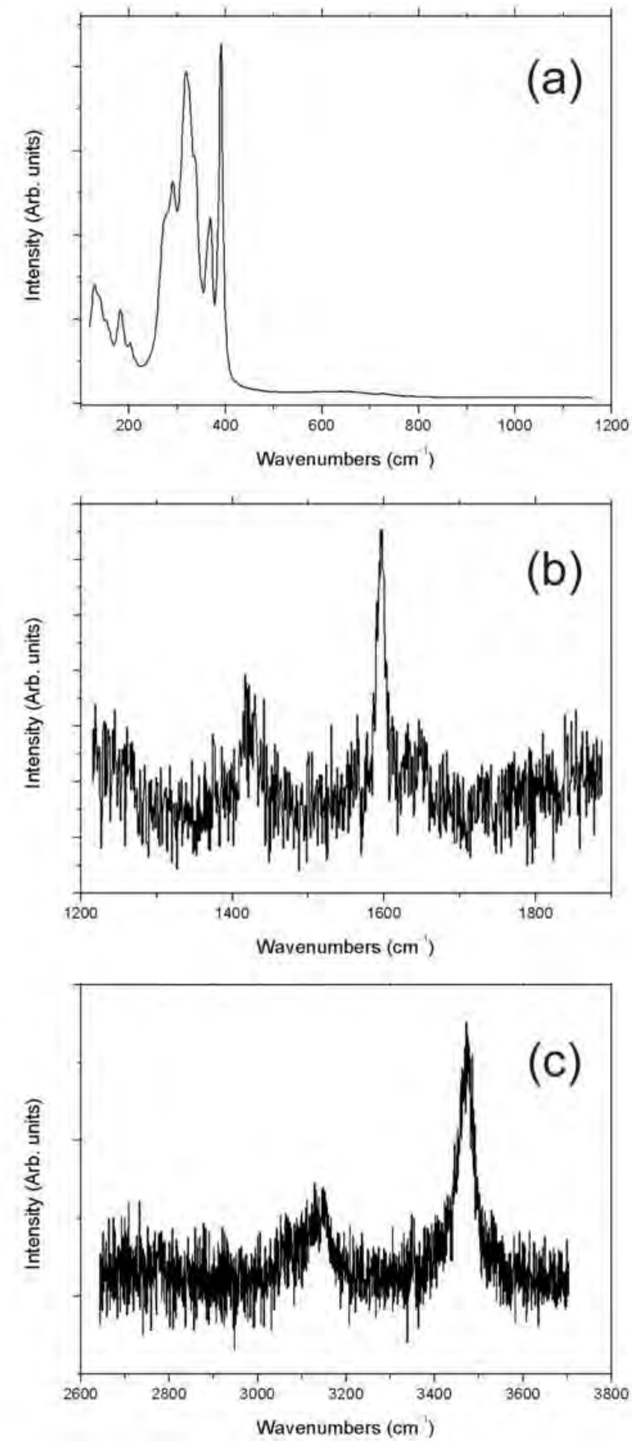

FIGURE 1. Raman spectra of ambrinoite.

(Laugier and Bochu 1999) are $a = 9.70(1)$, $b = 11.58(2)$, $c = 12.12(3)$ Å, $\alpha = 112.8(1)$, $\beta = 103.1(2)$, $\gamma = 90.7(2)°$, and $V = 1215(4)$ Å^3.

Single-crystal X-ray diffraction

Preliminary Weissenberg photographs suggested a triclinic symmetry and indicated that even very small fragments of ambrinoite actually consist of multiple crystals. However, it was possible to obtain the triclinic unit cell in a Bruker-AXS three circle diffractometer working with graphite monochromated Mo$K\alpha$ X-radiation and equipped with a Smart-Apex CCD detector. At room temperature, the triclinic unit cell was: $a = 9.716(1)$, $b = 11.581(1)$, $c = 12.103(2)$ Å, $\alpha = 112.71(1)$, $\beta = 103.48(1)$, $\gamma = 90.48(1)°$, and $V = 1214.3(3)$ Å^3.

The intensity data collection was performed at the Elettra synchrotron facility (Basovizza, Trieste, Italy) by using a very small crystal, with dimensions $0.08 \times 0.01 \times 0.005$ mm^3. Crystal data and experimental details are reported in Table 3. The wavelength of the radiation was set to 1.0 Å, and the crystal was placed at 36 mm from the 165 mm MarCCD detector. In this experimental setup, 73 frames were collected with a rotation angle $\Delta\varphi = 5°$. Data were integrated and corrected for Lorentz, polarization, and background effects using the HKL package (Otwinowski and Minor 1997) on the basis of the intensities of equivalent reflections. Reflections point to a triclinic cell, with $a = 9.704(1)$, $b = 11.579(1)$, $c = 12.102(2)$ Å, $\alpha = 112.82(1)$, $\beta = 103.44(1)$, $\gamma = 90.49(1)°$, and $V = 1211.6(3)$ Å^3. The a:b:c ratio calculated from the unit-cell parameters is 0.838:1:1.045. The solution and refinement of the structure were performed by means of the SHELX set of programs (Sheldrick 2008).

A Patterson map calculated in the space group $P\overline{1}$ revealed the coordinates of 12 electron density maxima, identified as Sb, As, and S on the basis of their heights and interatomic distances. The remaining atomic positions were deduced from difference Fourier syntheses. At this point, two couples of atoms, related by the inversion center, showed odd short distances, and the reliability index remained quite high (nearly 22%). After decreasing the symmetry to $P1$, the R index dropped to 10% and the difference Fourier map listed additional electron density maxima, which were attributed to H_2O molecules and to alkaline cations. After some least-square refinement cycles, in which anisotropic displacement parameters were introduced for all the atoms, and the ratio Sb/As was refined for the M sites, the refinement smoothly converged to $R_1 = 0.040$ for 2554 reflections with $F_o > 4\sigma(F_o)$ and 0.042 for all 2667 reflections. However, a careful scrutiny of the structure revealed that no deviations from a centrosymmetric atomic arrangement were present, and that a shift of the origin was needed to correctly describe the structure in the actual space group $P\overline{1}$. After a few cycles of refinement in this space group, and the refinement of the fraction of NH_4^+ substituting K^+ in the interlayer sites, the reliability index dropped to 0.035.

Atomic coordinates, occupation factors, and equivalent displacement parameters are shown in Table 4, anisotropic displacement parameters are listed in Table 5, whereas selected bond distances are reported in Table 6.

The refined occupancies for the M sites indicated that As and Sb statistically occupy M1 and M2 sites ($Sb_{0.54}As_{0.46}$ and $Sb_{0.57}As_{0.43}$, respectively), whereas the M5, M6, and M7 sites are mainly occupied by As with only minor Sb, and finally M3, M4, M8 are Sb-free (Table 4).

DESCRIPTION OF THE STRUCTURE

Cation coordination

M cations are bound exclusively to S, with the three shortest bonds ranging between 2.2 and 2.5 Å (Table 6). M1 and M2 sites, Sb-dominant, present the longest bond lengths (2.39 to 2.46 Å);

TABLE 2. X-ray powder diffraction for ambrinoite

h	*k*	*l*	d_{calc}†	I_{calc}‡	d_{obs}	I_{obs}§	*h*	*k*	*l*	d_{calc}†	I_{calc}‡	d_{obs}	I_{obs}§
0	0	1	10.784	100	10.7*	vs	$\bar{3}$	0	3	2.7302	6		
0	1	0	10.608	7			0	$\bar{4}$	3	2.7167	14	2.721*	mw
0	$\bar{1}$	1	9.769	8	9.6*	w	$\bar{1}$	$\bar{4}$	1	2.6927	5		
1	0	0	9.381	3			0	4	0	2.6520	4		
1	$\bar{1}$	0	7.446	2	7.4*	vw	$\bar{2}$	0	4	2.6482	23	2.646*	m
$\bar{1}$	$\bar{1}$	1	7.255	3	7.2*	vw	$\bar{1}$	2	3	2.6104	4		
1	1	0	6.672	10	6.7*	vw	3	2	0	2.5726	21	2.571*	m
0	1	1	6.390	6			2	0	3	2.5550	20		
1	$\bar{1}$	1	6.365	10			0	2	3	2.5401	3	2.537	s
1	0	1	6.322	10	6.29*	w	$\bar{3}$	2	2	2.5267	21		
$\bar{1}$	1	1	5.914	3			3	$\bar{2}$	2	2.4903	5	2.502	w
0	$\bar{1}$	2	5.845	5			$\bar{2}$	2	3	2.4903	6		
0	$\bar{2}$	1	5.761	52	5.75*	s	0	$\bar{4}$	4	2.4423	6		
$\bar{1}$	$\bar{1}$	2	5.527	6			$\bar{2}$	$\bar{4}$	3	2.4375	3	2.436	m
0	0	2	5.392	29	5.33	m	2	$\bar{4}$	0	2.4258	6		
$\bar{1}$	0	2	5.296	33			$\bar{4}$	0	1	2.4240	11		
$\bar{1}$	$\bar{2}$	1	4.9469	3			$\bar{3}$	$\bar{2}$	4	2.4116	6		
1	$\bar{2}$	1	4.8722	5	4.872*	w	2	2	2	2.4077	4		
1	$\bar{2}$	0	4.8515	4			$\bar{2}$	$\bar{4}$	1	2.3850	8	2.386*	w
$\bar{1}$	$\bar{2}$	2	4.5840	5	4.556*	w	0	4	1	2.3648	4	2.371*	vw
2	$\bar{1}$	0	4.4759	4			$\bar{3}$	0	4	2.3624	5		
$\bar{2}$	$\bar{1}$	1	4.4612	3			1	2	3	2.3190	3	2.329*	vw
1	0	2	4.2305	26	4.264*	mw	$\bar{2}$	4	1	2.2561	3	2.261*	w
0	2	1	4.1465	11	4.155*	m	3	3	0	2.2240	2	2.211*	vw
1	$\bar{2}$	2	4.1182	4			$\bar{1}$	2	4	2.1520	2	2.151*	vw
$\bar{1}$	2	1	4.0810	4			3	0	3	2.1074	7	2.123*	vw
2	0	1	3.9480	1	3.932*	vw	$\bar{2}$	$\bar{4}$	5	2.0869	3	2.089*	vw
0	$\bar{2}$	3	3.7558	29			2	$\bar{4}$	4	2.0591	3	2.064*	vw
2	$\bar{2}$	0	3.7229	10	3.721	m	$\bar{4}$	0	4	2.0480	1	2.047*	vw
0	$\bar{3}$	2	3.7182	3			$\bar{3}$	0	5	2.0353	5	2.039*	w
$\bar{1}$	0	3	3.6864	9			3	$\bar{4}$	3	1.9736	5	1.978*	w
$\bar{2}$	$\bar{2}$	1	3.6681	8								1.969	vw
$\bar{2}$	$\bar{2}$	2	3.6276	7	3.639	mw	$\bar{3}$	$\bar{4}$	5	1.9245	7		
2	$\bar{2}$	1	3.6073	5			0	$\bar{6}$	3	1.9203	4	1.922	mw
1	2	1	3.5577	4			$\bar{3}$	4	2	1.8965	3	1.898*	vw
0	3	0	3.5359	4	3.533*	vw	5	0	0	1.8762	4	1.870	w
1	$\bar{3}$	0	3.4360	1	3.435*	vw	$\bar{5}$	0	3	1.8711	5		
$\bar{2}$	0	3	3.2878	19	3.285*	m	$\bar{2}$	0	6	1.8432	6	1.845*	w
$\bar{1}$	2	2	3.2478	4			3	$\bar{4}$	4	1.8135	5	1.820*	vw
2	0	2	3.1610	26	3.170*	mw	0	0	6	1.7973	4	1.802	w
3	0	0	3.1270	11			2	0	5	1.7932	5		
$\bar{3}$	0	2	3.0667	16	3.075*	mw	0	2	5	1.7661	4	1.767	m
0	$\bar{4}$	2	2.8805	22			3	4	1	1.7660	7		
0	$\bar{4}$	1	2.8541	4	2.875	s	$\bar{3}$	4	3	1.7306	4	1.726*	vw
1	2	2	2.8412	5			$\bar{2}$	$\bar{4}$	7	1.6674	3	1.666*	w
3	0	1	2.8167	13			$\bar{3}$	$\bar{6}$	2	1.6180	5		
1	$\bar{4}$	1	2.7700	5			5	$\bar{4}$	0	1.6179	3	1.621	mw
$\bar{1}$	$\bar{4}$	2	2.7668	13			$\bar{3}$	6	0	1.6172	3		
$\bar{3}$	2	1	2.7525	5	2.762	s	$\bar{6}$	0	2	1.6163	7		
1	$\bar{4}$	2	2.7405	4			$\bar{5}$	$\bar{4}$	3	1.6054	3		

Notes: The asterisks indicate the 37 univocally indexed reflections, which were used to refine the unit cell. The experimental error is estimated to about 0.04 °2θ. This corresponds to an uncertainty in observed *d*-spacings in the order of magnitude of the last reported digit.
† The distances were calculated on the basis of the unit cell refined by using synchrotron data.
‡ Intensities were calculated on the basis of the structural model.
§ Observed intensities were visually estimated. s = strong; vs = very strong; m = medium; mw = medium-weak; w = weak, vw = very weak.

they form additional weak bonds with S13 and S12, respectively, at distances >2.90 Å. The other sites, M3 to M8, As-dominant, are characterized by shorter bond lengths, ranging from 2.198 Å (for M8, occupied exclusively by As) up to 2.376 Å for M6 site. M6 and M7 sites, in which up to 30 at% As is replaced by Sb, show an additional weak bond at ~3 Å.

K^+ and NH_4^+ occupy two sites, K1 and K2, with slightly different K/NH_4 s.o.f., 0.83/0.17 and 0.78/0.22, respectively. The smallest K1 site is eightfold coordinated; the shortest bond is formed with W1 (2.81 Å). The mean K1-S bond length is 3.40 Å. K2 site is 10-fold coordinated; the shortest bond is also with W1 (2.78 Å), while the mean bond length of the nine K2-S bonds is 3.598 Å.

Table 7 shows bond-valence analysis of cations and anions, according to Brese and O'Keeffe (1991). For K1 and K2 site, there is no bond valence parameter for NH_4^+-S bond, but, as NH_4^+ has almost the same size as Tl^+ (compare isotypic NH_4Cl and TlCl; Roberts et al. 2006), bond-valence balance was calculated considering NH_4^+ as Tl^+ and then using the known (Tl,S) and (Tl,O) parameters. This approach was applied recently by Zelenski et al. (2009), to infer indirectly the presence of minor NH_4^+ in a slightly expanded Pb site in the crystal structure of the complex sulfosalt tazieffite.

According to Table 7, the total bond valence of M atoms fits very well with the ideal value of 3 (from 2.89 to 3.07). While K1 shows also a good total (0.96), there is a significant lower total for K2 (0.87), which may be due to distinct sub-positions of NH_4^+ and K^+, whereas the crystal structure study gave only a mean position.

TABLE 3. Crystal data and summary of parameters describing data collection and refinement for ambrinoite

Crystal data	
X-ray formula	$[K_{1.61}(NH_4)_{0.39}]$ $(As_{6.36}Sb_{1.64})S_{13}\cdot H_2O$
Crystal size (mm^3)	$0.08 \times 0.01 \times 0.005$
Cell setting, space group	Triclinic, $P\bar{1}$
a, *b*, *c* (Å)	9.704(1), 11.579(1), 12.102(2)
α, β, γ (°)	112.82(1), 103.44(1), 90.49(1)
V ($Å^3$)	1211.6(3) $Å^3$
Z	2
Data collection and refinement	
Radiation, wavelength (Å)	synchrotron, λ = 1 Å
Temperature (K)	293
Detector to sample distance	36 mm
Active detection-area (cm^2)	16.5×16.5
Number of frames	73
Rotation width per frame (°)	5
Maximum observed 2θ	63.5
Measured reflections	9705
Unique reflections	2667
Reflections $F_o > 4\sigma(F_o)$	2554
R_{int} after absorption correction	0.0283
$R\sigma$	0.0234
Range of *h*, *k*, *l*	$-9 \leq h \leq 9$, $-12 \leq k \leq 12$, $-12 \leq l \leq 12$
R [F_o>4 σ F_o]	0.0341
R (all data)	0.0353
wR (on F_o^2)	0.0913
Goof	1.141
Number of least-squares parameters	225

TABLE 4. Atomic positions and equivalent displacement parameters for ambrinoite

Site	Site population	*x*	*y*	*z*	U_{eq}
M1	$Sb_{0.54}As_{0.46}$	0.39230(7)	0.64339(5)	0.83575(6)	0.0344(3)
M2	$Sb_{0.57}As_{0.43}$	0.01055(7)	0.14677(6)	0.83795(6)	0.0369(3)
M3	$As_{1.00}$	0.66142(10)	0.98014(7)	0.71276(7)	0.0309(3)
M4	$As_{1.00}$	0.66440(9)	0.70477(7)	0.70910(7)	0.0302(3)
M5	$As_{0.92}Sb_{0.08}$	0.24245(10)	0.92642(7)	0.96400(7)	0.0354(4)
M6	$As_{0.80}Sb_{0.20}$	0.00896(9)	0.64686(7)	0.82178(7)	0.0358(4)
M7	$As_{0.75}Sb_{0.25}$	0.38933(9)	0.14671(7)	0.82502(7)	0.0362(4)
M8	$As_{1.00}$	0.23678(10)	0.42874(8)	0.94031(8)	0.0365(3)
S1		0.6161(2)	0.7814(2)	0.5576(2)	0.0323(5)
S2		0.3786(2)	0.3401(2)	0.8069(2)	0.0404(5)
S3		0.8204(2)	0.0599(2)	0.6437(2)	0.0321(5)
S4		0.3974(2)	0.8510(2)	0.8382(2)	0.0371(5)
S5		0.4723(2)	0.5620(2)	0.6432(2)	0.0314(5)
S6		0.0114(2)	0.3439(2)	0.8169(2)	0.0367(5)
S7		0.8220(2)	0.5719(2)	0.6362(2)	0.0323(5)
S8		0.4694(2)	0.0630(2)	0.6408(2)	0.0348(5)
S9		0.1611(2)	0.0573(2)	0.6991(2)	0.0368(5)
S10		0.1587(2)	0.5625(2)	0.6931(2)	0.0345(5)
S11		0.0192(2)	0.8485(2)	0.8258(2)	0.0392(5)
S12		0.2637(2)	0.2992(2)	0.0350(2)	0.0398(5)
S13		0.2578(2)	0.7763(2)	0.0381(2)	0.0348(5)
K1	$K_{0.83}(NH_4)_{0.17}$	0.6680(3)	0.3331(2)	0.6791(3)	0.065(1)
K2	$K_{0.78}(NH_4)_{0.22}$	0.9242(4)	0.7592(3)	0.4774(3)	0.073(1)
W1	H_2O	0.2172(8)	0.7496(6)	0.5286(6)	0.066(2)

TABLE 5. Anisotropic displacement parameters for ambrinoite

	U_{11}	U_{22}	U_{33}	U_{23}	U_{13}	U_{12}
M1	0.0361(6)	0.0278(4)	0.0425(7)	0.0142(3)	0.0154(3)	0.0030(3)
M2	0.0341(6)	0.0298(4)	0.0500(5)	0.0192(3)	0.0109(3)	0.0023(3)
M3	0.0374(6)	0.0280(5)	0.0294(5)	0.0143(4)	0.0071(4)	0.0025(4)
M4	0.0369(7)	0.0269(5)	0.0280(5)	0.0135(4)	0.0062(4)	0.0012(4)
M5	0.0396(7)	0.0292(5)	0.0350(6)	0.0108(4)	0.0088(4)	0.0018(4)
M6	0.0327(7)	0.0285(5)	0.0451(6)	0.0143(4)	0.0087(4)	0.0024(3)
M7	0.0357(7)	0.0302(5)	0.0476(6)	0.0180(4)	0.0153(4)	0.0060(4)
M8	0.0409(7)	0.0282(5)	0.0377(5)	0.0110(4)	0.0091(4)	0.0014(4)
S1	0.044(1)	0.027(1)	0.027(1)	0.014(1)	0.005(1)	0.001(1)
S2	0.047(2)	0.033(1)	0.054(1)	0.024(1)	0.023(1)	0.006(1)
S3	0.031(1)	0.035(1)	0.031(1)	0.015(1)	0.006(1)	−0.002(1)
S4	0.044(2)	0.031(1)	0.045(1)	0.021(1)	0.017(1)	0.004(1)
S5	0.037(1)	0.029(1)	0.028(1)	0.010(1)	0.010(1)	−0.002(1)
S6	0.036(1)	0.032(1)	0.045(1)	0.021(1)	0.005(1)	0.004(1)
S7	0.033(1)	0.029(1)	0.031(1)	0.010(1)	0.005(1)	0.004(1)
S8	0.038(1)	0.041(1)	0.030(1)	0.018(1)	0.010(1)	0.011(1)
S9	0.035(1)	0.030(1)	0.040(1)	0.010(1)	0.012(1)	0.002(1)
S10	0.033(1)	0.032(1)	0.035(1)	0.008(1)	0.009(1)	0.001(1)
S11	0.039(1)	0.030(1)	0.049(1)	0.021(1)	0.001(1)	0.003(1)
S12	0.040(1)	0.053(1)	0.031(1)	0.023(1)	0.007(1)	0.005(1)
S13	0.042(1)	0.033(1)	0.030(1)	0.014(1)	0.009(1)	0.004(1)
K1	0.048(2)	0.058(2)	0.095(2)	0.044(2)	0.007(1)	0.003(1)
K2	0.088(3)	0.061(2)	0.075(2)	0.020(2)	0.044(2)	0.007(2)
W1	0.087(6)	0.046(4)	0.050(4)	0.014(3)	−0.004(3)	0.008(3)

Note: The anisotropic displacement factor exponent takes the form: $-2\pi^2[h^2a^{*2}U_{11} + ... + 2hka^*b^*U_{12}]$.

TABLE 6. Selected bond distances (Å)

M1 $Sb_{0.54}As_{0.46}$	–S4	2.392(2)	M2 $Sb_{0.57}As_{0.43}$	–S6	2.393(2)
	–S10	2.426(2)		–S9	2.418(2)
	–S5	2.463(2)		–S3	2.462(2)
	–S13	2.944(2)		–S12	2.962(2)
	–S12	3.281(2)		–S13	3.262(2)
	–S2	3.390(2)		–S11	3.402(2)
M3 $As_{1.00}$	–S8	2.253(2)	M4 $As_{1.00}$	–S5	2.254(2)
	–S3	2.260(2)		–S7	2.258(2)
	–S1	2.294(2)		–S1	2.288(2)
	–S13	3.150(2)		–S12	3.031(2)
M5 $As_{0.92}Sb_{0.08}$	–S13	2.236(2)	M6 $As_{0.80}Sb_{0.20}$	–S11	2.317(2)
	–S4	2.323(2)		–S10	2.321(2)
	–S11	2.327(2)		–S7	2.379(2)
				–S13	2.981(2)
				–S12	3.423(2)
				–S6	3.486(2)
M7 $As_{0.75}Sb_{0.25}$	–S2	2.334(2)	M8 $As_{1.00}$	–S12	2.198(2)
	–S9	2.339(2)		–S6	2.299(2)
	–S8	2.378(2)		–S2	2.307(3)
	–S12	3.009(2)			
	–S13	3.381(2)			
	–S4	3.490(2)			
K1 $K_{0.83}(NH_4)_{0.17}$	–W1	2.815(8)	K2 $K_{0.78}(NH_4)_{0.22}$	–W1	2.779(8)
	–S1	3.299(3)		–S1	3.334(4)
	–S6	3.338(3)		–S10	3.464(3)
	–S5	3.379(3)		–S6	3.500(4)
	–S7	3.400(3)		–S9	3.534(4)
	–S3	3.420(3)		–S3	3.571(4)
	–S8	3.474(3)		–S7	3.668(3)
	–S2	3.495(4)		–S2	3.736(4)
				–S9	3.770(4)
				–S11	3.806(4)

Note: The actual content of the M1–M8 and K1–K2 sites is reported.

General organization

Considering only the three shortest M-S bonds, the crystal structure of ambrinoite can be described on the basis of MS_3 triangular pyramids sharing S corners to form two types of chains $[(As,Sb)_4S_7]_\infty$ running along [100]; within each chain, trigonal pyramids arranged in M_3S_5 triangular groups alternate with a single MS_3 pyramid (Fig. 2a). The two different chains are connected each other by sharing the S corner of the single pyramids of each chain, giving rise to double chains $[(As,Sb)_8S_{13}]_\infty$ (Fig. 2b). In Figure 2c these double chains are seen along [100]. Two double chains are interpenetrated in a zigzag fashion into more complex columns forming layers parallel to (010). In ambrinoite, these layers are held together by (K, NH_4)-S bonds; H_2O molecules are coordinated by two K^+ cations, whereas K^+ cations are coordinated only by one H_2O, besides seven or nine S atoms. As the strong bonds, corresponding to short M-S bonds, occur exclusively within the complex columns, weak bonds between these columns could be easily broken: this explains the perfect {001} and {010} cleavages observed under the microscope. Two different orientations of the crystal structure of ambrinoite are

TABLE 7. Bond-valence balance in ambrinoite

	S1	S2	S3	S4	S5	S6	S7	S8	S9	S10	S11	S12	S13	W1	$\Sigma_{cations}$
M1		0.06		0.95	0.79					0.87		0.09	0.21		2.97
M2			0.80			0.97			0.90		0.06	0.21	0.09		3.03
M3	0.91		1.00					1.02					0.09		3.02
M4	0.93				1.02		1.00					0.12			3.07
M5				0.89							0.88		1.12		2.89
M6						0.04	0.82			0.96	0.97	0.05	0.16		3.00
M7		0.96		0.04				0.85	0.94			0.15	0.06		3.00
M8		0.88				0.90						1.18			2.96
K1	0.15	0.09	0.11		0.12	0.13	0.11	0.09						0.16	0.96
K2	0.14	0.05	0.09		0.08	0.09	0.06		0.04	0.10	0.04			0.18	0.89
Σ_{anions}	2.13	2.04	2.00	1.88	2.01	2.13	1.99	1.96	1.88	1.93	1.95	1.80	1.73	0.34	

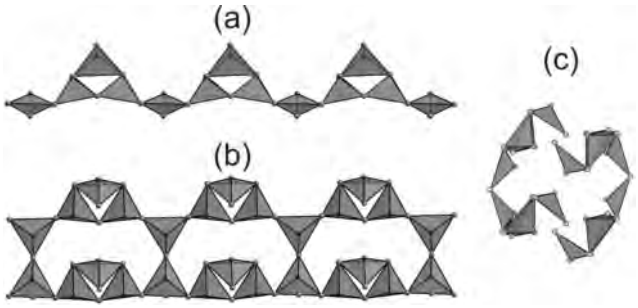

FIGURE 2. Chains of MS_3 pyramids in ambrinoite as seen: (**a**) down [010], **a** horizontal; (**b**) normal to (001), **a** horizontal; (**c**) down [100].

sketched in Figure 3.

Taking also into account the longer M-S bonds, the column layer becomes a complex slab with negative charge, $[(As,Sb)_8S_{13}]^{2-}$ (Fig. 4). Big, weakly bound cations $(K,NH_4)^+$, together with H_2O molecules, fill the inter-slab space that permits to relate ambrinoite structure in the field of solid-state chemistry to the family of intercalation compounds.

Ambrinoite as an OD structure

The structural refinement of ambrinoite allows us to recognize the details of its structural modules, at difference from what happens in the closely related sulfosalt gillulyite (Foit et al. 1995), which shows a high degree of disorder in both the shape of the chains formed by $(As,Sb)S_3$ pyramids, and the actual distribution of the Tl^+ cations between the chains. On the basis of the average structure refined by Foit et al. (1995), Makovicky and Balić-Žunić (1999) proposed two possible ordering models for gillulyite. Moreover, they used the OD theory to derive the four possible subcells of gillulyite (Table 1 in Makovicky and Balić-Žunić 1999), by stacking two different kinds of layers, one of them being disordered.

Also, the structure of ambrinoite can be described as built up by two kinds of layers, both of them ordered. From a geometric point of view, the inter-slab space above can be considered as a separate layer; the two kinds of layers are represented in Figure 5 and 6, respectively. The first one (denoted as "layer A," in agreement with the description of minerals belonging to the hutchinsonite merotypic family in Makovicky 2005) is formed by double chains of $(As,Sb)S_3$ pyramids and corresponds to a distorted slab $(110)_{PbS}$ of modified PbS archetype, whereas the second one ("layer B") is formed by K^+ and NH_4^+ cations and H_2O molecules.

The two layers have the same *a* and *b* parameters, namely *a*

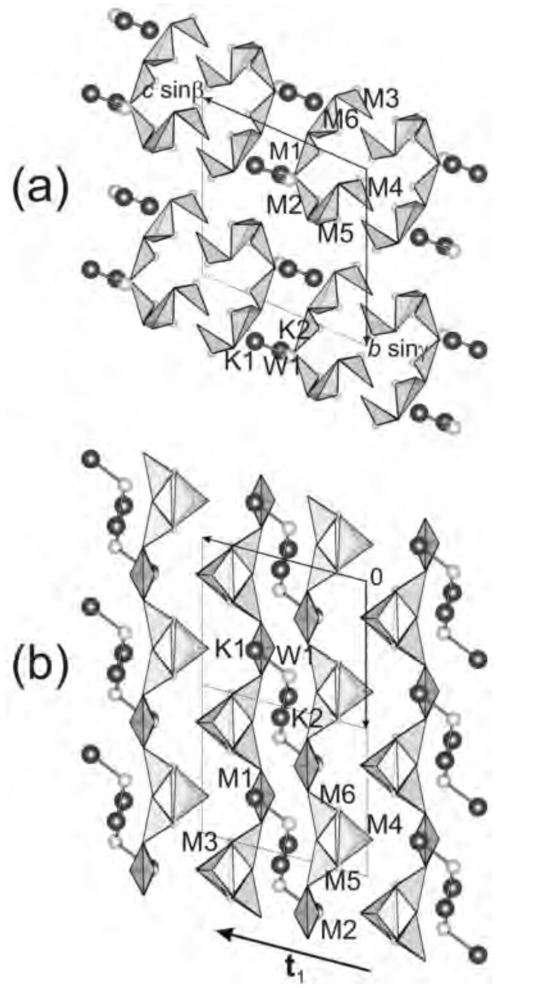

FIGURE 3. Crystal structure of ambrinoite as seen down [100] in (**a**) and down [010] in (**b**).

= 9.70 Å and b = 11.58 Å, and different widths: the layer group symmetry of the layer A is $P2_1/m1(1)$, whereas the layer group symmetry of layer B is $P11(\bar{1})$. The parentheses indicate the direction of missing periodicity.

The OD structure presents two distinct ρ-planes, which are both λ-ρ-planes, so that the structure belongs to the IV category (Ferraris et al. 2004). The OD groupoid family symbol for ambrinoite may be written as

$$P\ \ {}^{2_1}\!/_{m}\ \ 1\ \ (1) \qquad\qquad P\ \ 1\ \ 1\ \ (\bar{1})$$
$$\left[-0.147... \quad -0.203...\right]$$

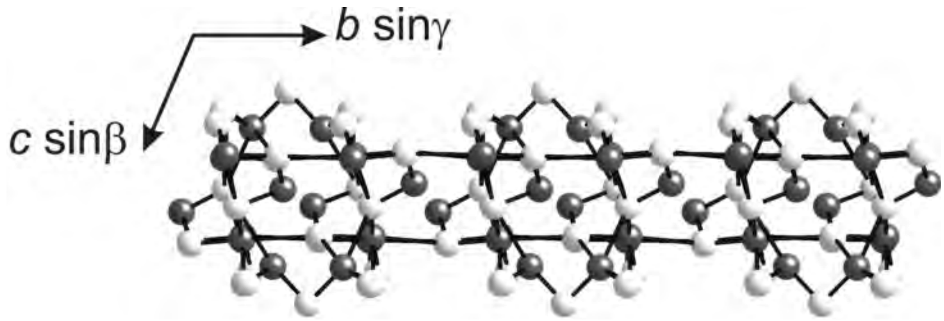

FIGURE 4. Ball and stick model of the complex slab $[(As,Sb)_8S_{13}]^{2-}$ in ambrinoite. Dark and white balls are (Sb,As) and S atoms, respectively.

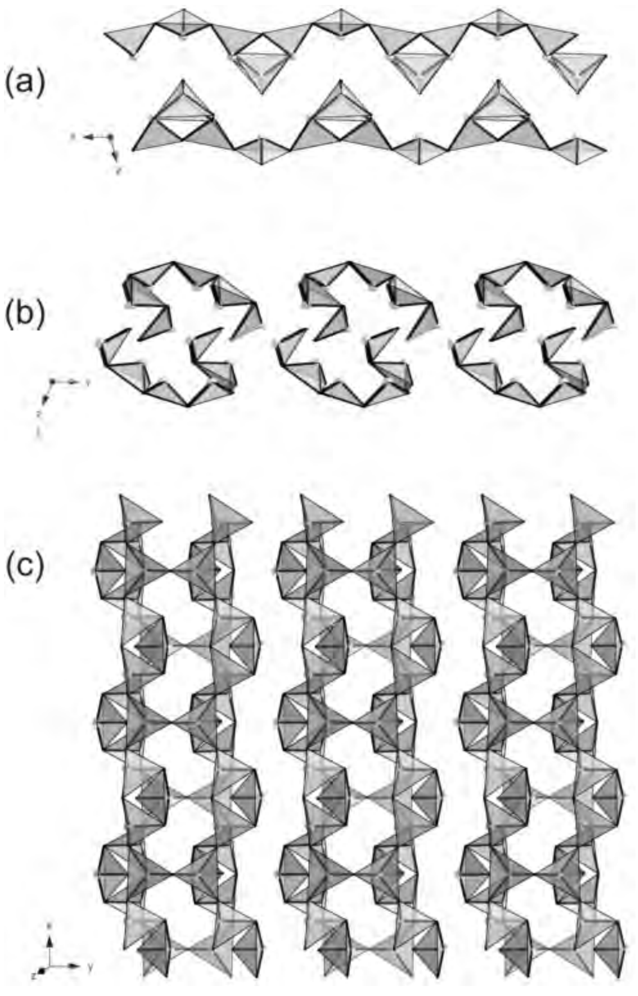

FIGURE 5. Layer A in three different orientations.

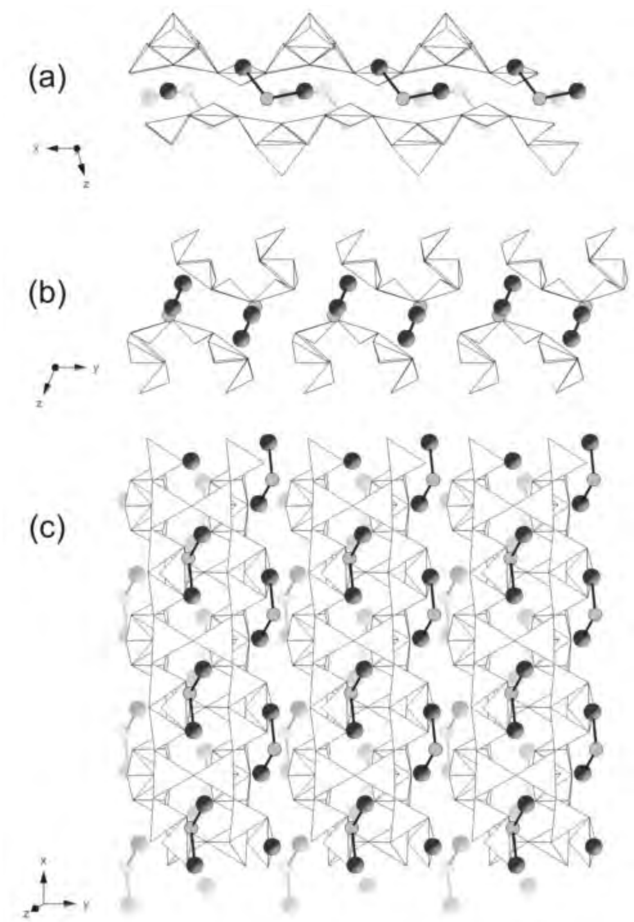

FIGURE 6. Layer B in three different orientations. Black and gray balls represent K cations and H_2O molecules, respectively. For sake of clarity, the MS_3 pyramids forming the layer A are outlined in white color.

where the numbers within square brackets are the *r* and *s* components of the projection of the vector connecting the origins of the two subsequent layers. The *r* and *s* values are referred to the common *a* and *b* translations, respectively.

If we assume an arbitrary position for the layer B_{2n}, the positions of the adjacent layers A_{2n-1} and A_{2n+1} are uniquely determined. They are related by the inversion center, which is a λ operation of the layer B. It means that only one variety of triples $A_{2n-1}B_{2n}A_{2n+1}$ exists. On the contrary, if we assume an arbitrary position for the layer A_{2n+1}, there are two possible positions for each of the adjacent layers B_{2n} and B_{2n+2}. Layers B_{2n} and B_{2n+2} can be related by either the 2_1 axis parallel to **a** or by the inversion center, both being λ operations of the A layer.

There are two possible structures that present only two kinds of triples of layers, and they are called polytypes with maximum degree of order (i.e., MDO polytypes) in the OD theory. To characterize them it is useful to introduce the concept of *generating operation*, namely the "τ-operation with a translational component parallel to the stacking direction, with magnitude equal to the distance between the two closest τ-equivalent layers" (Ďurovič 1997).

In the former MDO polytype (MDO_1), the inversion center in A is active. The generating operation is the translation $\mathbf{t}_1 = \mathbf{c}_0+2r\mathbf{a}+2s\mathbf{b}$, where c_0 = 10.78 Å corresponds to the distance between the two nearest-neighbor equivalent λ-planes, and *r* and *s* are defined above. The inversion center is valid for the whole structure, which is triclinic $P\bar{1}$, and has cell parameters a = 9.70, b = 11.58, c = 12.10 Å, α = 112.8, β = 103.4, and γ = 90.5°. It corresponds to the structure of ambrinoite, as described in the previous paragraphs and drawn in Figure 3.

In the second MDO polytype (MDO_2), the twofold screw axis 2_1 along [100] in the layer A is active. The constant application of this operation generates a monoclinic structure. Its generating operation is a glide normal to **a** with translation component $\mathbf{c}_0$, which becomes a glide *c* in a structure with $\mathbf{c} = 2\mathbf{c}_0+4s\mathbf{b}$. The corresponding structure has space group $P2_1/c11$, cell parameters a = 9.70, b = 11.58, c = 23.52 Å, α = 111.8°.

The observed X-ray diffraction patterns of ambrinoite do not show any indication about the occurrence of this MDO_2 polytype in our sample. However, it could occur in other crystals from the same or other possible localities.

Relationship with other natural or synthetic sulfosalts

In nature, alkaline sulfosalts are very rare: the two hydrated oxysulfosalts cetineite, $NaK_5Sb_{14}S_6O_{18}(H_2O)_6$ (Sabelli et al. 1988), and its dimorph ottensite, $Na_3(Sb_2O_3)_3(SbS_3)\cdot 3H_2O$ (Sejkora and Hyršl, 2007); galkhaite, $(Cs,Tl,\square)(Hg,Cu,Zn)_6(As,Sb)_4S_{12}$ (Divjaković and Nowacki 1975; Chen and Szymański 1981), and the hydrated Na sulfosalt, gerstleyite, $Na_2(Sb,As)_8S_{13}\cdot 2H_2O$ (Nakai and Appleman 1981). Ambrinoite is the first natural (K,NH_4)-hydrated sulfosalt.

According to its crystal structure, ambrinoite is the last discovered member of a wide group of natural and synthetic sulfosalts of As and/or Sb combined with large mono- or divalent cations (Tl^+, NH_4^+, Cs^+, Na^+, Pb^{2+}, Rb^+, organic cations), belonging to the hutchinsonite merotypic series (Makovicky 1997). The structures of these phases consist of regular 1:1 intergrowths of two kinds of slabs, one of which is common to all members, whereas the second one may differ.

Taking into account the chains of corner-sharing MS_3 pyramids, this kind of chain is already known to occur in two natural sulfosalts belonging to the hutchinsonite family: gillulyite, and gerstleyite. In particular, ambrinoite is strictly related to gillulyite, $Tl_2(As,Sb)_8S_{13}$, described by Wilson et al. (1991) from the Mercur gold deposit (Utah, U.S.A.). The crystal structure of gillulyite was determined by Foit et al. (1995) and reinterpreted, in the light of the order-disorder theory, by Makovicky and Balić-Žunić (1999). Considering one of the ordered polytypes (*P*-ordering) of gillulyite, hypothesized by the latter authors, the chains formed by MS_3 pyramids are topologically identical to those in ambrinoite; gillulyite differs from the latter in the substitution $Tl^+ = (K,NH_4)^+$ and in the absence of H_2O. Raman spectra collected during this work on a sample of gillulyite, with the aim to verify the presence of H_2O, did not show any evidence of the presence of this molecule. As in cetineite and gerstleyite, also in ambrinoite the H_2O molecules are bound only to the alkali cations. The MS_3 chains of ambrinoite and gillulyite are similar to that of gerstleyite; in this mineral, $(Sb,As)S_3$ pyramids are linked to form double chains, running along [100] (Nakai and Appleman 1981). However, whereas in gerstleyite (space group *Cm*) the single chains within the double ones are related by a mirror plane, such symmetry element is not present in ambrinoite and gillulyite.

In addition, several other synthetic sulfosalts show the same kind of MS_3 chains, i.e., $(NH_4)_2Sb_4S_7$ (Dittmar and Schäfer 1977), $[C_4H_8N_2][Sb_4S_7]$ (Parise and Ko 1992), $[C_2H_8N]_2[Sb_8S_{12}(S_2)]$ (Tan et al. 1996), and $Rb_2Sb_8S_{12}(S_2)\cdot 2H_2O$ (Berlepsch et al. 2001).

Other compounds with a similar stoichiometry were hydrothermally prepared by Wang et al. (2000), who described the synthesis and crystal structure of $[(CH_3NH_3)_{0.5}(NH_4)_{1.5}]Sb_8S_{13}\cdot 2.8H_2O$ and $Rb_2Sb_8S_{13.3}\cdot 3.3H_2O$. Even if they display a stoichiometry similar to that of ambrinoite, these two synthetic compounds show 12-membered rings of SbS_3 pyramids, linked into one-dimensional complex chains, very different from the crystal structure of ambrinoite.

As pointed out by Makovicky (2005), K is a "channel-building" element in sulfosalts; in fact, ambrinoite has a microporous character, with the presence of channels, filled with H_2O molecules and $(K,NH_4)^+$ cations, clearly underlining the zeolitic aspect of this new mineral phase.

Thus, ambrinoite constitutes the first natural sulfosalt with a significant content of ammonium, substituting about 1/4 of potassium atoms in the crystal structure. The crystal structure of ambrinoite is homeotypic with that of gillulyite. In the light of the present investigation and the work of Makovicky and Balić-Žunić (1999), ambrinoite, gillulyite and gerstleyite, belonging to the hutchinsonite merotypic series (Makovicky 1997; Moëlo et al. 2008), could be included in the new gerstleyite mineral group, according to the definition given by Mills et al. (2009). Following the Strunz classification (Strunz and Nickel 2001), ambrinoite belongs to the 2.HE subgroup (sulfosalts with alkalies and H_2O).

According to the original geochemistry revealed by the paragenesis described at Signols, the metallogenic process forming ambrinoite may be the result of the interaction of post-acid magmatism fluids generated within the crystalline basement, and bringing Li (in mica), B (in tourmaline), F (in fluorite), Cs (in galkhaite), As, Sb, and Tl (in sulfides and sulfosalts), with overlying Triassic formations, where reducing conditions due to organic matter favored a high ammonium concentration as well as the precipitation of sulfur as sulfides. These peculiar geochemical conditions may favor the discovery of other characteristic minerals at Signols.

Acknowledgments

We thank Pierluigi Ambrino, mineral collector, who provided us with the first samples of ambrinoite for study, and Marco Lezzerini for the measurement of micro-hardness. Thanks are also due to Bob Downs for the preliminary Raman test of the RRUFF specimen of gillulyite. Microprobe analysis was performed owing to the skilled advice of M. Bohn (CNRS engineer, Département Géosciences Marines, IFREMER, Centre de Brest). E.B. thanks Stefano Merlino for the helpful suggestions and discussions about the OD nature of ambrinoite and gillulyite. Both the referees, Francesco Demartin and Stefan Graeser, are warmly thanked for their constructive revision of the paper. This research was financially supported by MIUR through project PRIN 2007 "Compositional and structural complexity in minerals (crystal chemistry, microstructures, modularity, modulations): analysis and applications," and was made possible by the municipality of Oulx and the Department of Mineralogical and Petrological Sciences of the University of Torino, which allowed us to collect the investigated samples at the Signols quarry.

References cited

Berlepsch, P., Miletich, R., Makovicky, E., Balić-Žunić, T., and Topa, D. (2001) The crystal structure of synthetic $Rb_2Sb_8S_{12}(S_2)\cdot 2H_2O$, a new member of the hutchinsonite family of merotypes. Zeitschrift für Kristallographie, 216, 272–277.

Biagioni, C., Ciriotti, M.E., Ambrino, P., and Brizio, P. (2010) Secondo ritrovamento europeo di galkhaite, Cumbë Sûrdë, Signols, Piemonte. Micro (U.K. report), 1/2010, 124–129.

Bogomolov, G.V., Kudel'skiy, A.V., and Kozlov, M.F. (1970) The ammonium ion as an indicator of oil and gas. Doklady of the USSR Akademy of Sciences, Earth Science Section (English translation American Geological Institute), 195, 202–204.

Brese, N.E. and O'Keeffe, M. (1991) Bond-valence parameters for solids. Acta Crystallographica, B47, 192–197.

Broz, M.E., Cook, R.F., and Whitney, D.L. (2006) Microhardness, toughness, and modulus of Mohs scale minerals. American Mineralogist, 91, 135–142.

Chen, T.T. and Szymański, J.T. (1981) The structure and chemistry of galkhaite, a mercury sulfosalt containing Cs and Tl. Canadian Mineralogist, 19, 571–581.

Colomba, L. (1898) Ricerche mineralogiche sui giacimenti di anidrite e gesso dei dintorni di Oulx (Alta Valle della Dora Riparia). Atti della Reale Accademia delle Scienze di Torino, 33, 779–797.

——— (1909) Osservazioni mineralogiche e litologiche sull'alta Valle della Dora Riparia (Rocce e minerali della Beaume, Oulx). Rivista di Mineralogia e Cristallografia Italiana, 38, 35–82.

Damarco, P. and Barresi, A. (2005) I giacimenti gessiferi in Piemonte, p. 17–26. Gruppo Mineralogico e Paleontologico, CAI-UGET (Club Alpino Italiano-Unione Giovani Escursionisti Torinesi), Torino.

Dittmar, G. and Schäfer, M. (1977) Darstellung und Kristallstruktur von $(NH_4)_2Sb_4S_7$. Zeitschrift für anorganische und allgemeine Chemie, 437, 183–187.

Divjaković, V. and Nowacki, W. (1975) Die Kristallstruktur von Galchait $[Hg_{0.76}(Cu,Zn)_{0.24}]_{12}Tl_{0.96}(AsS_3)_8$. Zeitschrift für Kristallographie, 142, 262–270.

Ďurovič, S. (1997) Fundamentals of the OD theory. In S. Merlino, Ed., Modular Aspects of Minerals, 1, p. 3–28. European Mineralogical Union (EMU) Notes in Mineralogy, Eötvös University Press, Budapest.

Ferraris, G., Makovicky, E., and Merlino, S. (2004) Crystallography of Modular Materials, 370 pp. Oxford University Press, U.K.

Foit, F.F., Robinson, P.D., and Wilson, J.R. (1995) The crystal structure of gillulyite, $Tl_2(As,Sb)_8S_{13}$, from the Mercur gold deposit, Tooele County, Utah, USA. American Mineralogist, 80, 394–399.

Forneris, R. (1969) The infrared and Raman spectra of realgar and orpiment. American Mineralogist, 54, 1062–1074.

Frondel, C. and Morgan, V. (1956) Inderite and gerstleyite from the Kramer borate district, Kern County, California. American Mineralogist, 41, 839–843.

Guiguet, D., Gallizio, S., and Di Maio, M. (2003) Guida dei toponimi di Savoulx e Constans, 158 p. Alzani Editore, Pinerolo.

Huneau, B., Ding., J.J., Rogl, P., Bauer, J., Ding, X.Y., and Bohn, M. (2000) Experimental investigation in the quaternary systems Ti-Ni-Al-N and Ti-Ni-Al-O. Journal of Solid State Chemistry, 155, 71–77.

Kharbish, S., Libowitzky, E., and Beran, A. (2007) The effect of As-Sb substitution in the Raman spectra of tetrahedrite-tennantite and pyrargyrite-proustite solid solutions. European Journal of Mineralogy, 19, 567–574.

Korotkov, A.S. and Atuchin, V.V. (2008) Prediction of refractive index of inorganic compounds by chemical formula. Optics Communications, 281, 2132–2138.

Kraus, W. and Nolze, G. (2000) Powdercell 2.3. Bundesanstalt für Materialforschung und–prüfung, Berlin, Germany.

Laugier, J. and Bochu, B. (1999) CELREF: Cell parameters refinement program for powder diffraction diagram. Laboratoire des Matériaux et du Génie Physique, Ecole Nationale Supérieure de Physique de Grenoble (INPG), Grenoble, France.

Makovicky, E. (1997) Modular crystal chemistry of sulphosalts and other complex sulphides. In S. Merlino, Ed., Modular Aspects of Minerals, 1, p. 237–271. European Mineralogical Union (EMU) Notes in Mineralogy, Eötvös University Press, Budapest.

——— (2005) Micro- and mesoporous sulfide and selenide structures. In G. Ferraris and S. Merlino, Eds., Micro- and Mesoporous Mineral Phases, 57, p. 403–434. Reviews in Mineralogy and Geochemistry, Mineralogical Society of America, Chantilly, Virginia.

Makovicky, E. and Balić-Žunić, T. (1999) Gillulyite $Tl_2(As,Sb)_8S_{13}$: reinterpretation of the crystal structure and order-disorder phenomena. American Mineralogist, 84, 400–406.

Mills, S.J., Hatert, F., Nickel, E.H., and Ferraris, G. (2009) The standardisation of mineral group hierarchies: application to recent nomenclature proposals. European Journal of Mineralogy, 21, 1073–1080.

Moëlo, Y., Makovicky, E., Mozgova, N.N., Jambor, J.J., Cook, N., Pring, A., Paar, W., Nickel, E.H., Graeser, S., Karup-Møller, S., and others. (2008) Sulfosalt systematic: a review. Report of the sulfosalt sub-committee of the IMA Commission on Ore Mineralogy. European Journal of Mineralogy, 20, 7–46.

Nakai, I. and Appleman, D.E. (1981) The crystal structure of gerstleyite, $Na_2(Sb,As)_8S_{13}\cdot 2H_2O$, the first sulfosalt mineral of sodium. Chemistry Letters, 10, 1327–1330.

Otwinowski, Z. and Minor, W. (1997) Processing of X-ray diffraction data collected in oscillation mode. In C.W. Carter Jr. and R.M. Sweet, Eds., Methods in Enzymology, 276, p. 307–326. Macromolecular Crystallography, Part A, Academic Press, New York.

Parise, J.B. and Ko, Y. (1992) Novel antimony sulfides: synthesis and X-ray structural characterization of $Sb_3S_5\cdot N(C_3H_7)_4$ and $Sb_4S_7\cdot N_2C_4H_8$. Chemistry of Materials, 4, 1446–1450.

Pekov, I.V. and Bryzgalov, I.A. (2006) New data on galkhaite. New Data on Minerals, 41, 26–32.

Pironon, J., Pagel, M., Lévêque, M.H., and Mogé, M. (1995a) Organic inclusions in salt. Part I: Solid and liquid organic matter, carbon dioxide and nitrogen species in fluid inclusions from the Bresse basin (France) Organic Geochemistry, 23, 391–402.

Pironon, J., Pagel, M., Walgenwitz, F., and Barrès, O. (1995b) Organic inclusions in salt. Part 2: oil, gas and ammonium in inclusions from the Gabon margin. Organic Geochemistry, 23, 739–750.

Polino, R., Ed. (1999) Note illustrative della carta geologica d'Italia alla scala 1:50000. Bardonecchia. Servizio Geologico d'Italia, Roma, 76 p.

Roberts, A.C., Venance, K.E., Seward, T.M., Grice, J.D., and Paar, W.H. (2006) Lafossaite, a new mineral from the La Fossa crater, Vulcano, Italy. Mineralogical Record, 37, 165–168.

Sabelli, C., Nakai, I., and Katsura, S. (1988) Crystal structure of cetineite and its synthetic analogue $Na_{3.6}(Sb_2O_3)_3(SbS_3)(OH)_6\cdot 2.4H_2O$. American Mineralogist, 73, 398–404.

Sejkora, J. and Hyršl, J. (2007) Ottensite: a new mineral from Qinglong, Guizhou Province, China. Mineralogical Record, 38, 77–81.

Sheldrick, G.M. (2008) A short history of SHELX. Acta Crystallographica, 64, 112–122.

Strunz, H. and Nickel, E.H. (2001) Strunz Mineralogical Tables, 9th ed., 870 p. E. Schweizerbart'sche Verlagsbuch-handlung, Stuttgart, Germany,

Tan, K., Ko, Y., Parise, J.B., Park, J.-H., and Darovsky, A. (1996) A novel antimony sulfide templated by dimethylammonium: its synthesis and structural characterization using synchrotron/imaging plate data. Chemistry of Materials, 8/10, 2510–2515.

Wang, X., Liu, L., and Jacobson, A.J. (2000) Hydrothermal synthesis and crystal structures of $[(CH_3NH_3)_{0.5}(NH_4)_{1.5}]Sb_8S_{13}\cdot 2.8H_2O$ and $Rb_2Sb_8S_{13}\cdot 3.3H_2O$. Journal of Solid State Chemistry, 155, 409–416.

Wilson, J.R., Robinson, P.D., Wilson, P.N., Stanger, L.W., and Salmon, G. (1991) Gillulyite, $Tl_2(As,Sb)_8S_{13}$, a new thallium arsenic sulfosalt from the Mercur gold deposit, Utah. American Mineralogist, 76, 653–656.

Zelenski, M., Garavelli, A., Pinto, D., Vurro, F., Moëlo, Y., Bindi, L., Makovicky, E., and Bonaccorsi, E. (2009) Tazieffite, $Pb_{20}Cd_2(As,Bi)_{22}S_{50}Cl_{10}$, a new chlorosulfosalt from Mutnovsky volcano, Kamchatka Peninsula, Russian Federation. American Mineralogist, 94, 1312–1324.

Manuscript received October 15, 2010
Manuscript accepted January 26, 2011
Manuscript handled by Andrew McDonald